Fibers and Polymers (2024) 25:891–900
https://doi.org/10.1007/s12221-023-00451-x

Online ISSN 1875-0052
Print ISSN 1229-9197

REGULAR ARTICLE

Superhydrophobic and Photocatalytic Self-Cleaning Cotton Fabrics Coated with SiO_2–TiO_2 Janus Particles and PDMS

Hongyang Wang[1] · Haiyang Yu[2] · Junsheng Wang[1] · Ting-Ting Li[2] · Jia-Horng Lin[2] · Ching-Wen Lou[2]

Received: 20 May 2023 / Revised: 17 November 2023 / Accepted: 1 December 2023 / Published online: 30 January 2024

Abstract

Cotton fabrics are susceptible to contamination in daily use. Herein, this study developed a scalable and benign strategy to impart superhydrophobic and photocatalytic properties to cotton fabrics by impregnating SiO_2–TiO_2 Janus particles (SiO_2–TiO_2 JPs) and silicone elastomer polydimethylsiloxane (PDMS). SiO_2–TiO_2 Janus particles were synthesized by Pickering template method. The obtained cotton fabrics exhibited good superhydrophobic properties with a water contact angle (WCA) of 155° as well as mechanical and chemical stability. The modified fabrics maintained their superhydrophobic properties against 30 cycles of mechanical abrasion, 15 cycles of tape peeling, and 24 h of UV aging. They also had good resistance to n-hexane, acetone, acid/alkali liquids. The degradation efficiency of Rhodamine B (RhB) was up to 63% after 6 h of UV irradiation and still 48% after 5 cycles of degradation. The facile approach in favor of large-scale preparation showed promising potential for wide application of flexible, superhydrophobic cotton fabrics with self-cleaning performance.

Keywords Self-cleaning · Janus particles · Superhydrophobic properties · Photocatalytic

1 Introduction

Cotton fabrics are widely used in apparel, household textiles, and automotive trim due to their softness, breathability, low cost, and environmental friendliness. However, cotton fabrics are easily wetted and contaminated by liquids such as coffee and milk due to the numerous hydrophilic groups (-OH) on cellulose fibers. The introduction of superhydrophobic coatings can overcome these problems simply and effectively [1–3].

The surface with lotus effect has a large water contact angle ($\theta_{CA} > 150°$) and a small water sliding angle (WSA, $\theta_{SA} < 10°$) [4–6]. In the past 20 years, methods have been used to prepare artificial superhydrophobic surfaces, including vapor deposition, layer-by-layer assembly, hydrothermal, tessellation, chemical etching, photolithography, wrinkling, etc. [7–13]. Wang et al. deposited alumina particles onto low surface energy vulcanized silicone rubber to obtain superhydrophobic coatings with self-cleaning effect and investigated the droplet bounce under different conditions [14]. Liu et al. grew silicon carbide nanowires on the surface of mullite fabrics by simple impregnation and in situ polymerization, and modified them with dopamine and octadecylamine to produce superhydrophobic coatings with excellent mechanical wear resistance and chemical stability [15]. Although the above superhydrophobic materials showed good repellency to a wide range of liquids, such as water and coffee, they did not block contamination by oily liquids. Li et al. prepared superhydrophobic fabrics with excellent robustness, washing durability, and self-healing ability by sequentially spraying SiO_2 aerogel particles modified by fluorosilane (FAS) and polyvinylidene fluoride-hexafluoropropylene (PVDF-HFP) onto cotton fabrics. The treated fabrics were still repellent to lower surface tension liquids such as soybean oil and ethylene glycol [16]. Jiao et al. prepared superamphiphobic coatings by spraying fluorinated SiO_2 and ceramic binders. Among them, the modified SiO_2 was embedded inside the coating in agglomerated capsules and could be released to the surface after wear, which had some self-healing characteristics. In addition, droplets of motor oil, n-decane,

✉ Ching-Wen Lou
cwlou@asia.edu.tw

Hongyang Wang
wanghongyang@tfri.com.cn

[1] Tianjin Fire Science and Technology Research Institute of MEM, Tianjin 300381, China

[2] Innovation Platform of Intelligent and Energy-Saving Textiles, School of Textile Science and Engineering, Tiangong University, Tianjin 300387, China

hexadecane, cyclohexane, and soybean oil could be maintained in a stable Cassia–Baxter state on the surface [17]. However, long-chain perfluoroalkyl materials are expensive and difficult to biodegrade, posing a potential environmental risk.

Photocatalysis is a simple and effective method to overcome the above disadvantages. In recent years, the combination of photocatalysis and superhydrophobicity has attracted much attention due to its excellent self-cleaning properties [18–22]. Wang et al. prepared fluorine-free superhydrophobic cotton fabrics by in situ growth of TiO_2 and grafting hydrophobic octadecyl methacrylate (ODMA) chain segments using thiol-olefin click reactions. The superhydrophobic cotton fabrics showed a photodegradation rate of 98.0% for methyl blue in 120 min, and the degradation rate still reached more than 97.0% after 5 cycles [23]. Wang et al. first prepared fly ash-titanium dioxide (FA-TiO_2) core–shell particles, followed by grafting PDMS chain segments under UV irradiation, and finally mixed with PDMS to impregnate the fabrics to prepare various superhydrophobic materials. The treated fabrics were self-extinguishing after 7 s of ignition due to the flame retardancy of the FA in them. In addition, the superhydrophobic effect was restored by irradiating the dodecane contaminated cotton fabrics with UV light. After 36 contamination cycles, the superhydrophobic properties were maintained [24]. However, the photocatalytic effect can also damage the substances with low surface energy loaded on the fiber surface, and degrade some of the hydrophobic chain segments grafted on the nanoparticles. These effects will promote the generation of surface hydroxyl groups, causing a gradual decrease of superhydrophobic properties [25–27]. This problem has not yet received much attention.

Janus particles (JPs) are two different functions combined on their opposite sides. They are named after the two-faced god Janus in Roman mythology. The term "Janus beads" was first used in 1988 by Casagrande et al. to describe the behavior of amphiphilic beads at the oil–water interface. In terms of material composition, JPs can be divided into three main categories: soft (organic, polymer-based), hard (inorganic, metal), and mixed organic/inorganic JPs [28]. In terms of shape, they can be divided into columnar, raspberry, flaky, spherical, and so on [29–32]. In terms of properties, they can be classified into acidic and basic, amphiphilic, magnetically responsive, etc. [33, 34]. Bao et al. prepared superhydrophobic coatings by spraying polyurethane and amphiphilic Janus particles onto leather sequentially. The amino groups on the hydrophilic side of the Janus particles reacted with the isocyanate groups on the polyurethane layer to crosslink, thus enhancing the mechanical fastness of the coating [33]. However, Janus particles are mainly used in emulsion stabilization, catalysis, biomedicine, etc. [35–37].

In this paper, superhydrophobic cotton fabrics with photocatalysis capability were prepared via a simple impregnation method. First, Janus particles with photocatalytic activity were synthesized by the Pickering emulsion method and later added to PDMS to obtain a mixed solution for impregnating cotton fabrics. The coated cotton fabrics showed outstanding superhydrophobicity property and were promising for self-cleaning application. The superhydrophobic cotton fabrics also demonstrated mechanical durability, UV-durability and anti-corrosion. The above results indicate that the prepared superhydrophobic cotton fabrics with photocatalysis capability in this study expands the application of self-cleaning Janus particles in textile fields.

2 Experimental

The woven cotton fabrics (127 g/m^2) were purchased from Jinzhou Shunlongfa Textile Co., Ltd. Hydrochloric acid (37%) and sodium hydroxide (96%) were supplied by Tianjin Fengchuan Chemical reagent Co., LTD. Dodecyl trimethoxysilane (DTMS, 93%) was supplied by Shanghai Xianding Biotechnology Co., LTD. Ethyl orthosilicate (TEOS, 98%) was supplied by Kermel. Tetrabutyl titanate (TBOT, 99%) was obtained from Aladdin; 3-aminopropyltriethoxysilane (APTES, 99%), n-heptane (98%), petroleum ether (bp 60–90 ℃) was supplied by Macklin. Paraffin wax (mp 62–64 ℃), hydroxyethyl cellulose (HEC), and ammonia (28%) were obtained from Rhawn. PDMS Dow Corning 184 and curing agent were supplied by Dow Corning.

2.1 Synthesis and Preparation

2.1.1 Synthesis and Modification of SiO_2 Particles

SiO_2 was synthesized via the Stöber method [38]. First, 0.5 mL of ethyl orthosilicate was dissolved in 2 mL of ethanol and added to a mixture of 100 mL of ethanol and 25 mL of ammonia and stirred for 2 h. Then, 8 mL of ethyl orthosilicate dissolved in 32 mL of ethanol was added to the previous seed solution. The final product was centrifuged at 9000 rpm, washed several times with ethanol, and dried at 80 ℃ for 24 h. 2 g of silica was dispersed in 100 mL of ethanol, followed by the addition of excess APTES to the ethanol solution and condensation reflux at 80 ℃ for 24 h.

2.1.2 Synthesis of Janus Particles

As shown in Fig. 1, surface-modified silica particles were used to construct Pickering emulsions with oil-in-water. 0.2 g of modified silica was sonicated and dispersed in 20 mL of deionized water for preparing the aqueous phase. Then 2 g of paraffin wax was added to the aqueous phase as the oil phase. After the paraffin wax melted at 80 ℃, a stable oil-in-water emulsion was formed by magnetic stirring at

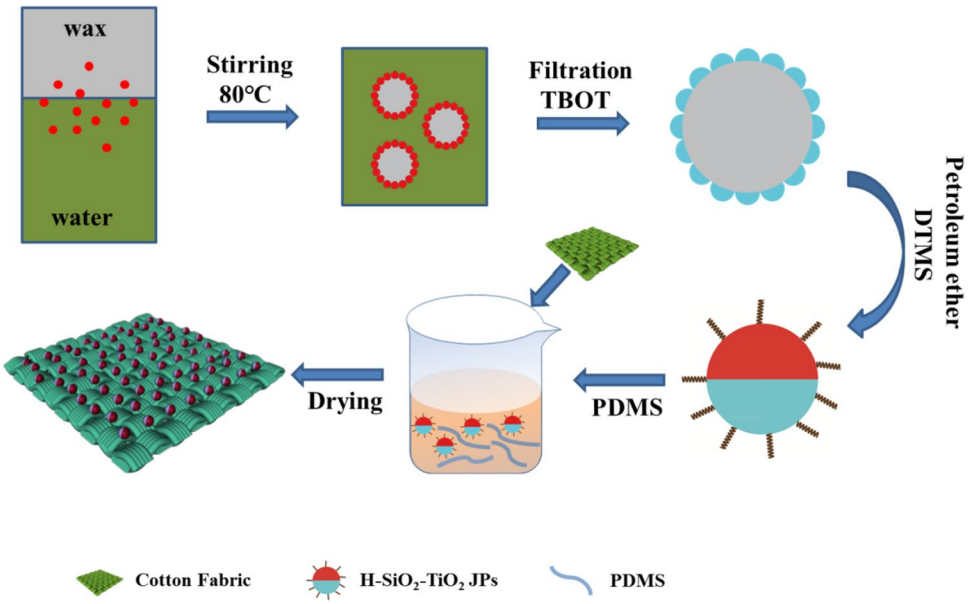

Fig. 1 Synthesis process of JPs and preparation of superhydrophobic cotton fabrics

1000 rpm for 1 h. The emulsion was placed in ice water and cooled down rapidly. After cooling down, the emulsion was filtered under vacuum and dried under vacuum at 30 ℃ for 12 h. 3 g of wax-SiO_2 was dispersed into 20 mL of ethanol, 0.075 g of HEC, and 0.2 mL of deionized water were added and stirred for 20 min. 1.0 g of TBOT was dissolved in 5 mL of ethanol, and the above solution was added drop by drop within 5 min. Then, the solution was stirred rapidly at 40 ℃ for 3 h, centrifuged at 9000 rpm, washed with ethanol, and the process was repeated twice. The wax (SiO_2–$TiO_{2)}$ was removed from paraffin with petroleum ether at 80 ℃ and calcined at 450 ℃ for 3 h. 1 g of SiO_2–TiO_2 JPs was dispersed in 100 mL of ethanol, pH adjusted to 2–4 by hydrochloric acid, 0.5 mL of DTMS, and 1 mL of deionized water were added and stirred in a water bath at 60 ℃ for 5 h. The samples were then centrifuged and washed to obtain hydrophobic SiO_2–TiO_2 JPs (H–SiO_2–TiO_2 JPs). After removing 3 g of paraffin semi-coated NH_2-SiO_2 from the paraffin, approximately 0.3 g of NH_2-SiO_2 was obtained. Therefore, 0.3 g of NH_2-SiO_2 was used to prepare TiO_2-coated SiO_2 pellets (SiO_2–TiO_2 Ps) according to the above method.

2.1.3 Preparation of the Superhydrophobic Cotton Fabrics

The cotton fabrics were desized with a 10 g/L alkali solution, and then ultrasonic washing with deionized water was carried out. A certain amount of H–SiO_2–TiO_2 JPs (0.7 wt%, 2.2 wt%, and 3.7 wt%), PDMS prepolymer (3.7 wt%, 5.1 wt%, and 6.6 wt%) and curing agent (10:1) were dissolved in 20 mL of n-heptane. After being stirring well, the cotton fabrics (3 × 3 cm) were immersed for 2 h, dipped and rolled, and cured at 80 ℃ for 5 h. The superhydrophobic cotton fabrics (SCF) with H–SiO_2–TiO_2 JPs and PDMS were named as HSCF. In addition, 0.1 mL DTMS was added to 10 mL ethanol, and then 0.1 g SiO_2, SiO_2–TiO_2 Ps, and SiO_2–TiO_2 JPs were added, respectively, and stirred for 2 h. The cotton fabrics were immersed in the above mixed solution and stirred for 30 min. Then, the cotton fabrics were heated in an oven at 80 ℃ for 5 h to obtain three different superhydrophobic cotton fabrics (SCF-1, SCF-2, and SCF-3).

2.1.4 Characterization

The samples were analyzed using Fourier transform infrared (FTIR, Thermo Scientific Nicolet iS20, USA) and X-ray photoelectron spectrometer (XPS, Thermo Fisher K-Alpha, USA) for functional groups. The morphology of the samples was observed by thermal field scanning electron microscopy (SEM Gemini SEM500, Germany). The wettability of the superhydrophobic fabrics was measured by contact angle measurement (JC2000DM, China) at room temperature. Photocatalytic activity was measured on a UV3600 spectrophotometer (UV3600, China). WCA and WSA values are the average of five measurements. 5 μL water droplets were used for WCA measurements and 10 μL water droplets were used for WSA measurements [39].

The durability of the superhydrophobic coatings was assessed using sandpaper abrasion and tape peel. For sandpaper abrasion, coated fabrics were placed on a sheet of 800-grit sandpaper at a constant pressure of 100 g and pulled horizontally for 10 cm in five cycles, and the WCA was recorded. For the tape peel test, the tape was tightly adhered to the fabrics and then removed. The stability of the coating was examined in different harsh environments. The fabrics were soaked in ethanol, hexane, acetone, acid (pH 2) and alkali (pH 12) for 24 h, rinsed with deionized water, dried

and tested for WCA. UV endurance tests were performed by placing the fabrics in a UV aging light box for 24 h continuous exposure.

To evaluate the photocatalytic activity, 100 mg of SiO_2–TiO_2 JPs, H–SiO_2–TiO_2 JPs powder, and 2 × 3 cm of superhydrophobic cotton fabrics were added to 100 mL of RhB dye solution (10 mg/L), respectively, and a xenon lamp (with a 420 nm cut-off filter, 500 W) was turned on as the UV light source. At regular intervals, 3 mL of the dye solution was removed, and the dye concentration was measured at 550 nm using a UV–visible spectrophotometer. The coated fabrics were wetted with ethanol before the test. The degradation efficiency is defined as (1-C/C_0), where C_0 indicates the initial concentration of pollutant, and C indicates the pollutant concentration at different time.

3 Results and Discussion

3.1 Characterization of the Synthesized Janus Particles

Janus particles were fabricated from SiO_2 particles via a combination of silane coupling agent modification and colloidal fabrication. The morphology of SiO_2 particles was as shown in Fig. S1. The SiO_2 particles were highly dispersed and had a diameter of (525 ± 20) nm. The amino-modified SiO_2 was used to stabilize the oil-in-water Pickering emulsion, and after the emulsion cooled down, NH_2-SiO_2 encapsulated paraffin colloids were formed, resulting in partial masking of NH_2-SiO_2. Using the sol–gel method, TiO_2 grew on the unmasked side of NH_2-SiO_2 and was calcined to give it some photocatalytic activity, as shown in Fig. 2. Thus, SiO_2–TiO_2 JPs with chemical anisotropy were prepared, as shown in Fig. 2c and Figure S2. The amino-modified SiO_2 embedded on the colloidal surface (Fig. 2a and b) was further modified by TBOT. As shown in Fig. 2c, the smooth side was SiO_2 and the rough side was TiO_2. TEM micrographs further confirmed that SiO_2–TiO_2 Janus particles with a particle size of approximately 600 nm were formed on the surface of SiO_2 partially supported by TiO_2.

Figure 3a (i) shows the XPS full spectrum of H-SiO_2–TiO_2 JPs. Figure 3 (a)(ii), (iii), and (iv) shows the high-resolution XPS spectra of O, Ti, and Si, respectively. Figure 3 (a)(ii) shows that the O 1 s high-resolution spectra could be fitted to three peaks at 539.20 eV, 531.34 eV, and 529.98 eV. They correspond to the Si–O bond, the Si–O-Ti bond, and the Ti–O bond, respectively [40]. Figure 3 (a)(iii) shows the high-resolution spectrum of Ti 2p, the peaks at 464.42 eV, 458.72 eV correspond to the binding energies of Ti $2p_{1/2}$ and Ti $2p_{3/2}$, respectively. Figure 3a(iv) shows that Si 2p could be fitted to two peaks at 103.50 eV and 101.69 eV, which correspond to the Si–O bond and the Si–O–Ti bond, respectively. The above results indicate that SiO_2 and TiO_2 are not simply physically combined, but through covalent bonds. This may be due to the formation of Si–O–Ti bonds on the surface of H–SiO_2–TiO_2 JPs by dehydration and condensation of hydroxyl groups.

Figure 3b shows the X-ray diffractograms of SiO_2 and SiO_2–TiO_2 JPs, respectively. It could be seen from the diffractograms that SiO_2 had a broad peak near 2θ = 22.4°, reflecting the properties of the amorphous material. However, SiO_2–TiO_2 JPs had distinct peaks at 2θ = 25.7°, 38.2°, 48.3°, 54.0°, 55.3°, and 63.0°, which correspond to the crystalline surfaces of anatase (101), (004), (200), (105), (211), and (204), respectively [41]. The results show that the anatase TiO_2 was generated in an internal structure of SiO_2–TiO_2 JPs. In addition, the characteristic peaks of the amorphous SiO_2 almost disappear. This is because the surface of SiO_2 has been partially covered by TiO_2.

FTIR was used to analyze the functional groups on the surface of the samples [42]. Figure 3c represents the FTIR spectra of SiO_2–TiO_2 JPs and H- SiO_2–TiO_2 JPs. In the spectra of SiO_2–TiO_2 JPs, the peaks at 1105 cm^{-1} and 797 cm^{-1} were due to the antisymmetric and symmetric stretching vibrations of Si–O-Si, respectively. The absorption bands near 1624 cm^{-1} and 956 cm^{-1} reflected the bending vibrations of Si–OH [40]. In the H- SiO_2–TiO_2 JPs spectrum, the peaks at 2922 cm^{-1} and 2854 cm^{-1} were caused by –CH_3 and –CH_2–, respectively. Comparing the two particles, the peaks of –CH_3 and –CH_2- indicate the successful hydrophobic modification of SiO_2–TiO_2 JPs by DTMS. The inset in

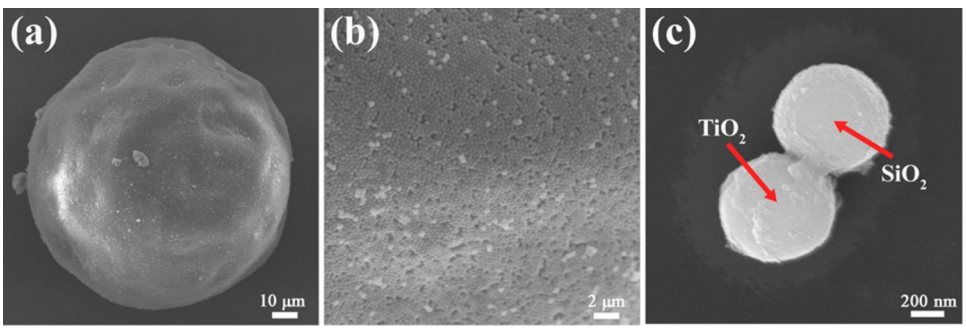

Fig. 2 **a**, **b** SEM images of the colloidosome. **c** SEM Images of SiO_2–TiO_2 JPs

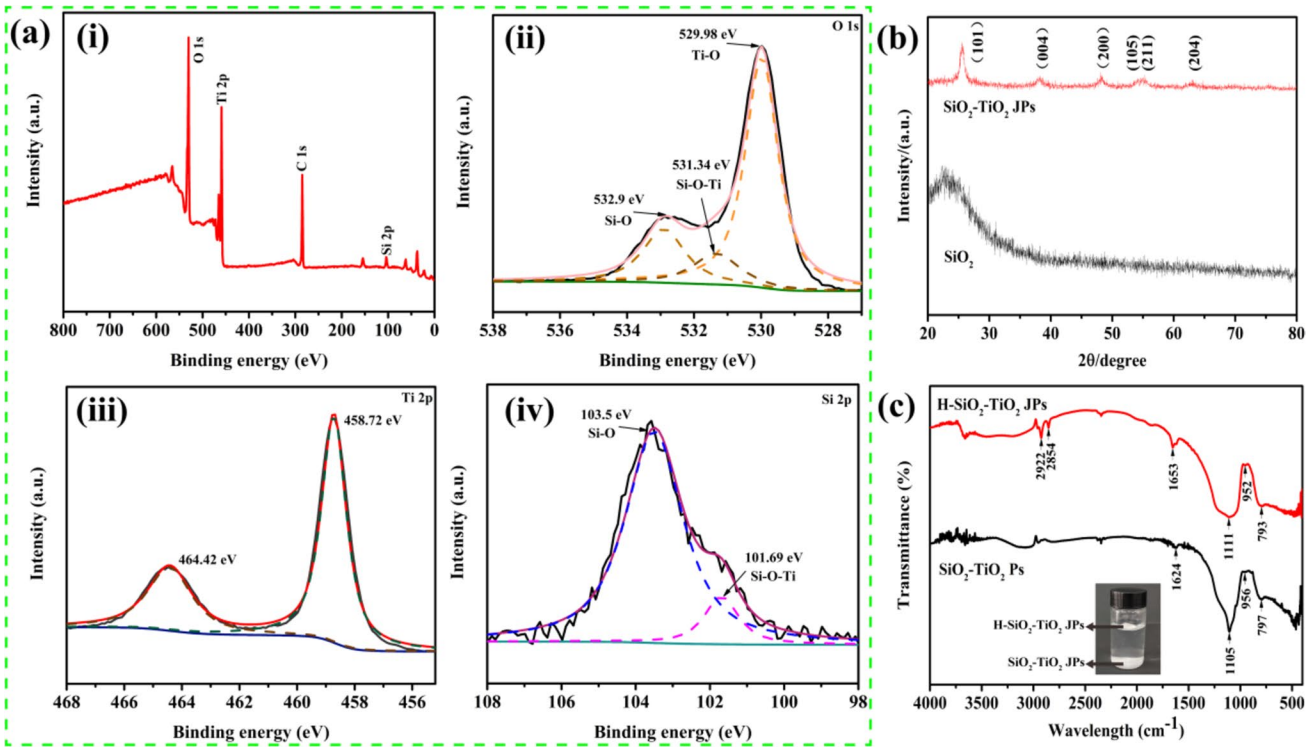

Fig. 3 **a** XPS spectra of H–SiO_2–TiO_2 JPs (i) Full-scan XPS spectra, (ii) O 1 s, (iii) Ti 2p and (iv) Si 2p spectra. **b** XRD patterns of SiO_2 and SiO_2–TiO_2 JPs. **c** FTIR spectra of SiO_2–TiO_2 JPs and H–SiO_2–TiO_2 JPs

Fig. 3(c) also shows that H- SiO_2–TiO_2 JPs float on the water due to their hydrophobicity.

3.1.1 Characterization of Superhydrophobic Fabrics

First, the differences between SiO_2–TiO_2 JPs, SiO_2–TiO_2 Ps, and SiO_2 particles in applications were explored, and the corresponding coated fabrics were prepared. However, the superhydrophobic properties of the coated fabrics gradually disappeared under shorter UV irradiation time. The corresponding results and discussions could be found in Fig. S3. To further increase the UV stability of the coating, the superhydrophobic cotton fabrics were prepared by choosing PDMS with better chemical stability mixed with SiO_2–TiO_2 JPs [43]. The construction of micro- and nanoscale rough structures is one of the keys to prepare superhydrophobic materials. Usually, the greater the roughness is, the better the superhydrophobicity. Therefore, the effect of the amount of H- SiO_2–TiO_2 JPs and PDMS on the surface morphology and wettability of the coated fabrics was investigated. It can be seen from Figure S4 that all coated fabrics reached 150°. However, the WCA varied with the content of different components. When 3.7 wt% of PDMS was added, the corresponding WCA kept increasing with the increase of H- SiO_2–TiO_2 JPs content, which was attributed to the construction of micro-/nano-structures on the fabric surface and the increase of roughness. When 3.7 wt% of H- SiO_2–TiO_2 JPs was added, the WCA kept decreasing with the increase of PDMS. This is because larger composite nanoparticles formed on the surface of cotton caused the agglomeration effect. When 2.2 wt% of H- SiO_2–TiO_2 JPs was added, the WCA first increased and then decreased with the increase of PDMS, with a maximum of 154.82°. This is again due to the excessive amount of PDMS, which led to the decrease in roughness. In summary, 2.2 wt% H- SiO_2–TiO_2 JPs and 5.1 wt% PDMS were selected as the best conditions for the preparation of superhydrophobic fabrics, and the following fabrics in this paper were prepared with this parameter.

The surface morphology and distribution features of PDMS and Janus particles on the surface of coating fabrics were explored by using SEM and EDS mapping images. Figure 4 shows the SEM images and corresponding WCA images of the pure cotton fabrics, PDMS-modified fabrics and Janus particle coated fabrics. As shown in Fig. 4a–c, the cotton fibers had smooth surface, and the WCA was 0°. On the other hand, the PDMS-coated fabrics had a slightly wavy surface with a WCA of 143°. When 0.1 g of H–SiO_2–TiO_2 JPs and 0.5 g of PDMS were added, the WCA of Janus particle coated fabrics was 152° and the superhydrophobic state was achieved. This is a result of increasing the roughness of the fiber surface by the Janus particles, as confirmed in Fig. 4c. The elemental composition of the fabric surface, as

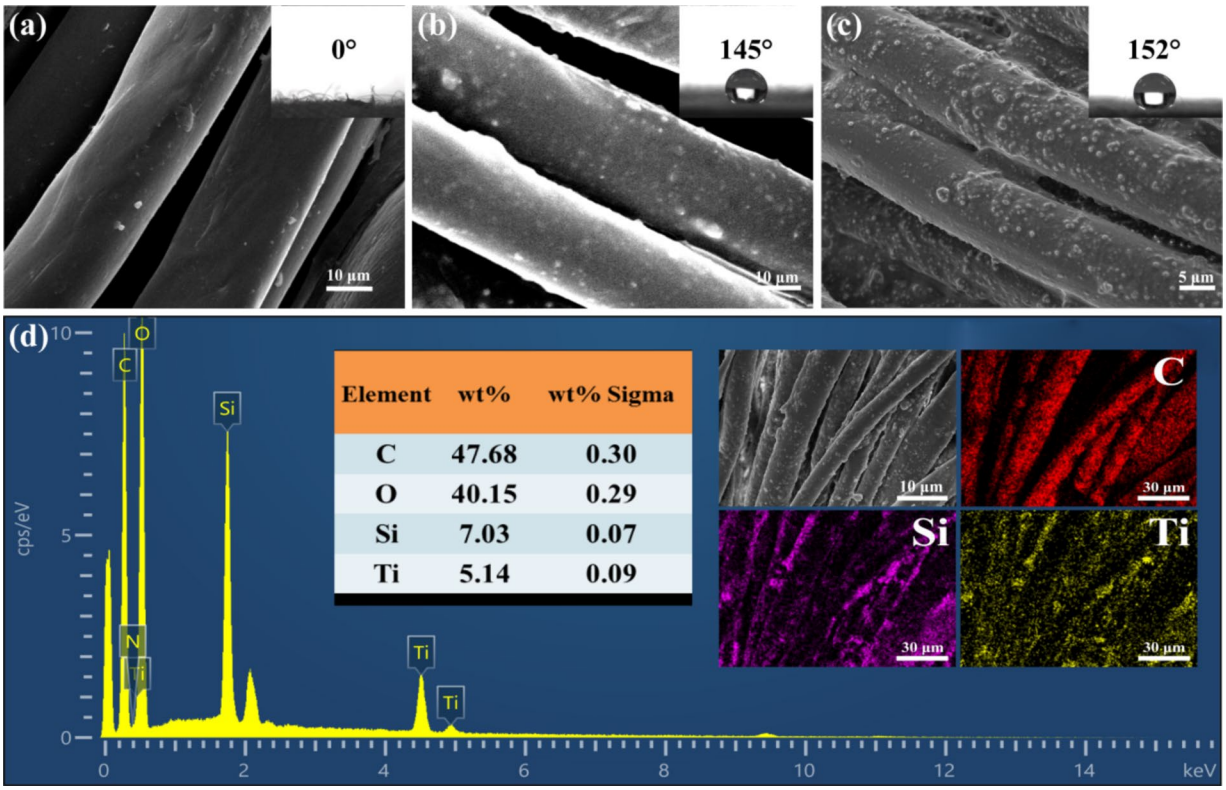

Fig. 4 SEM images of different fabrics of **a** CF, **b** PDMS-CF, **c** HSCF; **d** EDS images of HSCF

shown in Fig. 4d, contains four elements: C, O, Si, and Ti. The weight percentages of Ti and Si elements were 5.14% and 7.03%, respectively, indicating that the H–SiO_2–TiO_2 JPs and PDMS were uniformly distributed on the surface of the coated fabric.

In addition, it can be seen in Figure S5 that the characteristic peaks at 3311 cm^{-1} and 1711 cm^{-1} were caused by hydroxyl stretching and bending vibrations. The new characteristic peaks at 2963 cm^{-1} for HSCF were caused by –CH and at 798 cm^{-1} and 457 cm^{-1} were caused by Si–O-Si [44]. For HSCF, the significant decreased of the characteristic peaks at 3311 cm^{-1} and 1711 cm^{-1} and the new characteristic peak at 2963 cm^{-1} indicated the successful hydrophobic modification of the fabric.

3.1.2 Superhydrophobic Behaviors on HSCF

Figure 5 demonstrates the superhydrophobic properties of the fabrics. As shown in Fig. 5a, droplets of milk, coffee, juice, methylene blue-dyed water, hydrochloric acid at pH 2 and sodium hydroxide solution at pH 12 all stand on the surface of the fabrics in spherical shapes. This indicates that the modified fabrics exhibits superhydrophobic properties for a variety of liquids. Figure 5b indicates that when the cotton fabrics were immersed in water, an air layer was formed on the surface of the fabrics, producing a mirror-like shine, which was the result of water forming a Cassie–Baxter state on the surface of the fabrics. Figure 5(c) shows the state diagram of the droplet on the syringe needle when it was in contact with the fabric surface, which well indicated the adhesion of the droplet into the fabric surface. The needle carried the droplet in contact with the fabrics and squeezed the fabrics, and the droplet deformed. After that, the needle moved up, and the droplet came out of the fabrics with it. It could be found that the droplet did not wet the fabrics even when it was squeezed and deformed on the fabric surface, indicating that the coated fabrics had low adhesion to water. The self-cleaning performance of the superhydrophobic surface means that the droplets roll off from the fabric surface and take away the contaminants, such as dust, that are attached to it at the same time. In this study, carbon black particles were used as contaminants, adhered to the fabric surface, and rinsed with water to test its self-cleaning performance. As shown in Fig. 5d, the droplets became spherical without wetting the fabrics or even bounce off the fabric surface. As the droplets flow through the carbon black, they wrap the carbon black and adhere to it, sliding off the inclined fabric surface. After a period of rinsing, the fabric surface was rinsed clean, indicating that it has good self-cleaning performance.

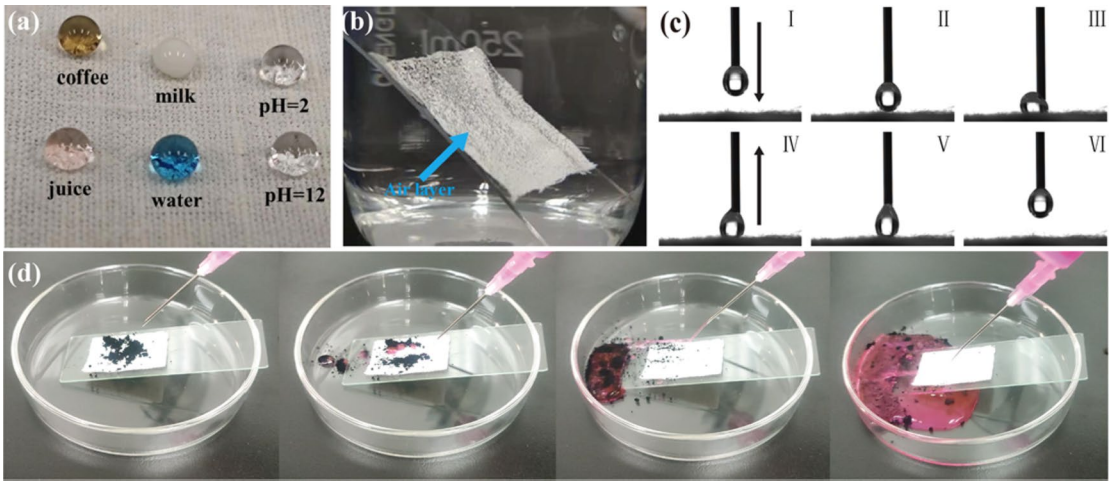

Fig. 5 **a** Photos of different liquid drops on the fabric surface; **b** photographs of fabrics immersed in water; **c** the process diagram of water drop and deformation on the fabric surface; **d** effect images of fabric self-cleaning

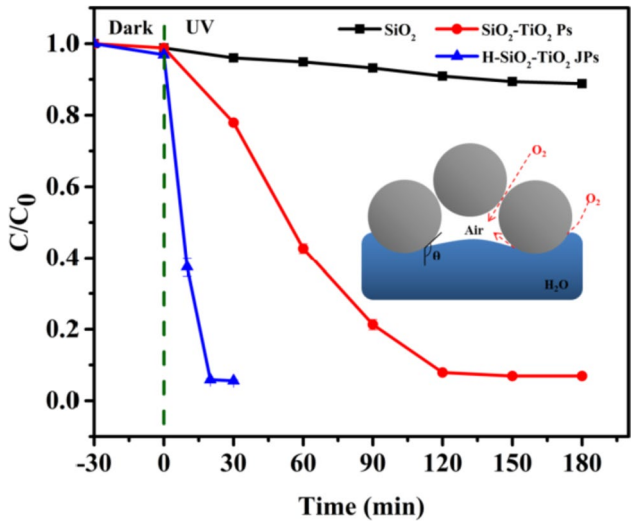

Fig. 6 Photocatalytic degradation effect of SiO_2–TiO_2 JPs and other samples on RhB

3.1.3 Photocatalytic Degradation

The photocatalytic performance of H–SiO_2–TiO_2 JPs can directly affect the photocatalytic efficiency of HSCF. Figure 6 shows the photocatalytic performance of different samples. In the dark reaction stage, the C/C_0 of the suspensions of the different added samples decreased slightly, indicating that they had basically no adsorption effect on rhodamine B. However, the degradation efficiency of different sample suspensions on RhB under UV light varied greatly. After UV irradiation for 180 min, the C/C_0 of SiO_2 suspensions decreased slightly, indicating that SiO_2 had no photocatalytic activity. Compared with SiO_2, the photocatalytic activity of SiO_2–TiO_2 JPs was much better. The degradation efficiency of SiO_2–TiO_2 JPs for RhB was up to 92% when UV irradiation was done for 120 min. This result indicates that SiO_2–TiO_2 JPs have good photocatalytic activity. Interestingly, due to the excellent hydrophobic property of H–SiO_2–TiO_2 JPs, they mostly float on the surface of RhB diluent. Although, the H–SiO_2–TiO_2 JPs cannot be fully mixed and contacted with the RhB diluent, they accumulate into a particle layer on the surface of the RhB diluent. The protruding part of the particle layer will contact with the RhB diluent and form an air–water interface. This gas–liquid–solid three-phase system makes full use of UV light and has a sufficient oxygen supply to generate more $\cdot O_2^-$ and ·OH, which enhance the photocatalytic efficiency [45, 46]. When H–SiO_2–TiO_2 JPs were added, the RhB concentration could be reduced by 94% within 20 min.

The degradation ability of RhB under UV light was used to assess the photocatalytic activity of the modified fabrics. Figure 7a shows the degradation of pure cotton fabrics and modified fabrics under UV light. It could be seen that the pure cotton fabrics were almost not degraded by RhB after 6 h of UV irradiation. While the degradation efficiency of modified fabrics for RhB in 6 h could reach 63%. The degradation principle is that TiO_2 on the fabric surface produces electron and hole under the light condition, and part of electron and hole migrate to the active sites on the photocatalyst surface, where electron could react with the H^+ and O_2 adsorbed on the TiO_2 surface for reduction to produce H_2, $\cdot O_2^-$, H_2O_2, etc.; hole with the H_2O and OH^- adsorbed on the TiO_2 surface to produce the more active oxide species ·OH, after which the active species is involved in the degradation reaction of RhB [47]. In addition, 20 μL of RhB solution was utilized to wet the coated fabrics for testing with photocatalytic degradation. As could be seen in the inset of Fig. 7a, the red color on the fabrics largely faded after 3 h.

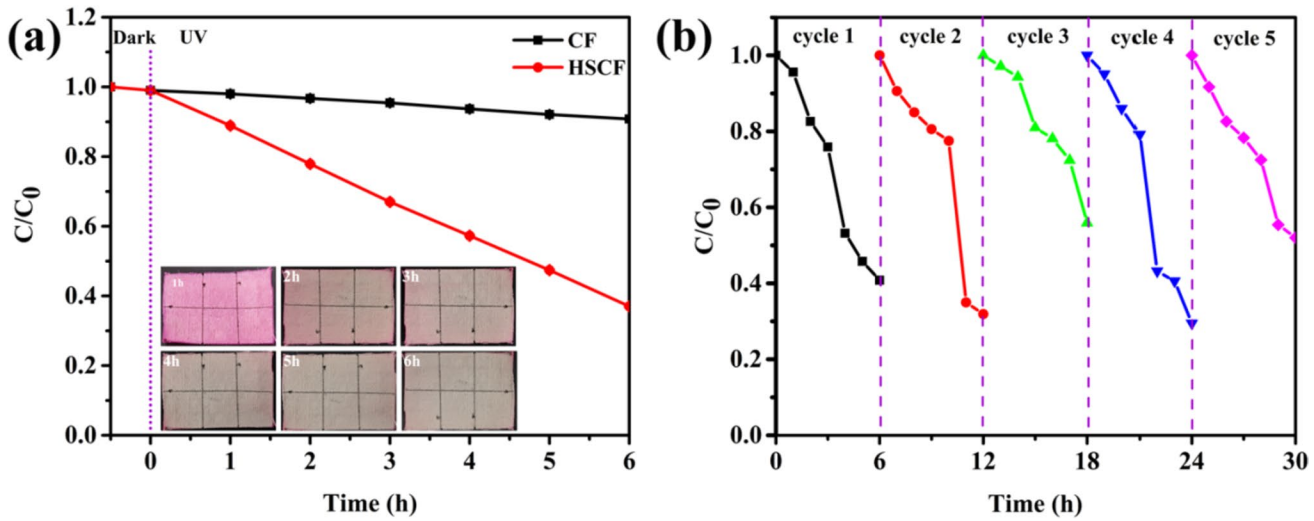

Fig. 7 **a** Photocatalytic degradation performance of different fabrics; repeated degradation of fabrics under UV irradiation

In summary, the modified fabrics had some photocatalytic activity. In addition, exploring the change in photocatalytic degradation efficiency of the modified fabrics through cyclic experiments is an important indicator of its practical application ability. Figure 7b shows the degradation activity of the modified fabrics on RhB. After five cycles of degradation, the degradation efficiency was 48% in 6 h, which was lower than the first 60%, but still had some photocatalytic degradation ability. As shown in Table S1, the HSCF coatings exhibited excellent photocatalytic degradation performance compared to previous superhydrophobic photocatalytic coatings.

3.1.4 Mechanical Stability and Environmental Durability

The stability properties of superhydrophobic materials are important in practical applications. In this study, a series of stability performance tests were performed on the modified fabric surfaces. In order to investigate the mechanical wear resistance of the fabric surface, weight rubbing and tape peeling tests were conducted, respectively. As can be seen in Fig. 8a, the WCA slowly decreased and the WSA rapidly increased as the number of tape peelings increases. After the 15th time, the WCA was less than 150°, and the superhydrophobicity was lost. In contrast to the fully particle covered surface in Figure S3, after 20 cycles of tape peeling, the surface particles of the fabrics were heavily shed, as shown in Fig. 8a. The WSA rose too fast because it depended on the adhesion of the fabric surface. Once the particles started to fall off and the roughness decreased, the adhesion of the fabrics increased rapidly. As can be seen in Fig. 8b, the WCA slowly decreased at 0–30 friction but was still higher than 150°. Continuing to rub the fabrics, it gradually lost its superhydrophobicity. In 0–40 rubles, it rose to 30°. As can be seen from the illustration in Fig. 8b, the fabric surface particles were sparse, but not as large as the damage caused by the tape peeling. As shown in Table S2, the HSCF coating has good mechanical durability and stability compared to previous superhydrophobic coatings.

When the fabrics were impregnated in ethanol, hexane, acetone, pH 2 hydrochloric acid solution, and pH 12 sodium hydroxide solution for 24 h, respectively, as in Fig. 8c, their contact angles were still greater than 150°. However, the WCA decreased slightly more in the hydrochloric acid solution at pH = 2, and this may be attributed to the fact that the acid damaged the surface coating of the fabrics, making the number of hydroxyl groups increase. However, in general, the stability of the coated fabrics against various organic solutions, acid and alkali was strong. As can be seen in Fig. 8d, the WCA of the fabrics was greater than 153° after 24 h of UV aging. The results indicated that the fabrics had excellent UV stability. This was attributed to the fact that the surface of the fiber and part of the particle surface were wrapped in PDMS, and the particles were sufficiently modified by DTMS. Therefore, there was no excessive increase of hydroxyl groups on the particle surface, and the superhydrophobicity was maintained.

4 Conclusion

In conclusion, superhydrophobic cotton fabrics with photocatalysis capability were successfully prepared by simply impregnating a mixture of H-v JPs and PDMS. H–SiO_2–TiO_2 JPs provided the photocatalytic effect and built the rough structure for the coating, and PDMS reduced the surface energy. When 2.2 wt% of H–SiO_2–TiO_2 JPs and 5.1 wt% of PDMS were added, the superhydrophobic cotton fabrics obtained had a high WCA of about 155°. In addition,

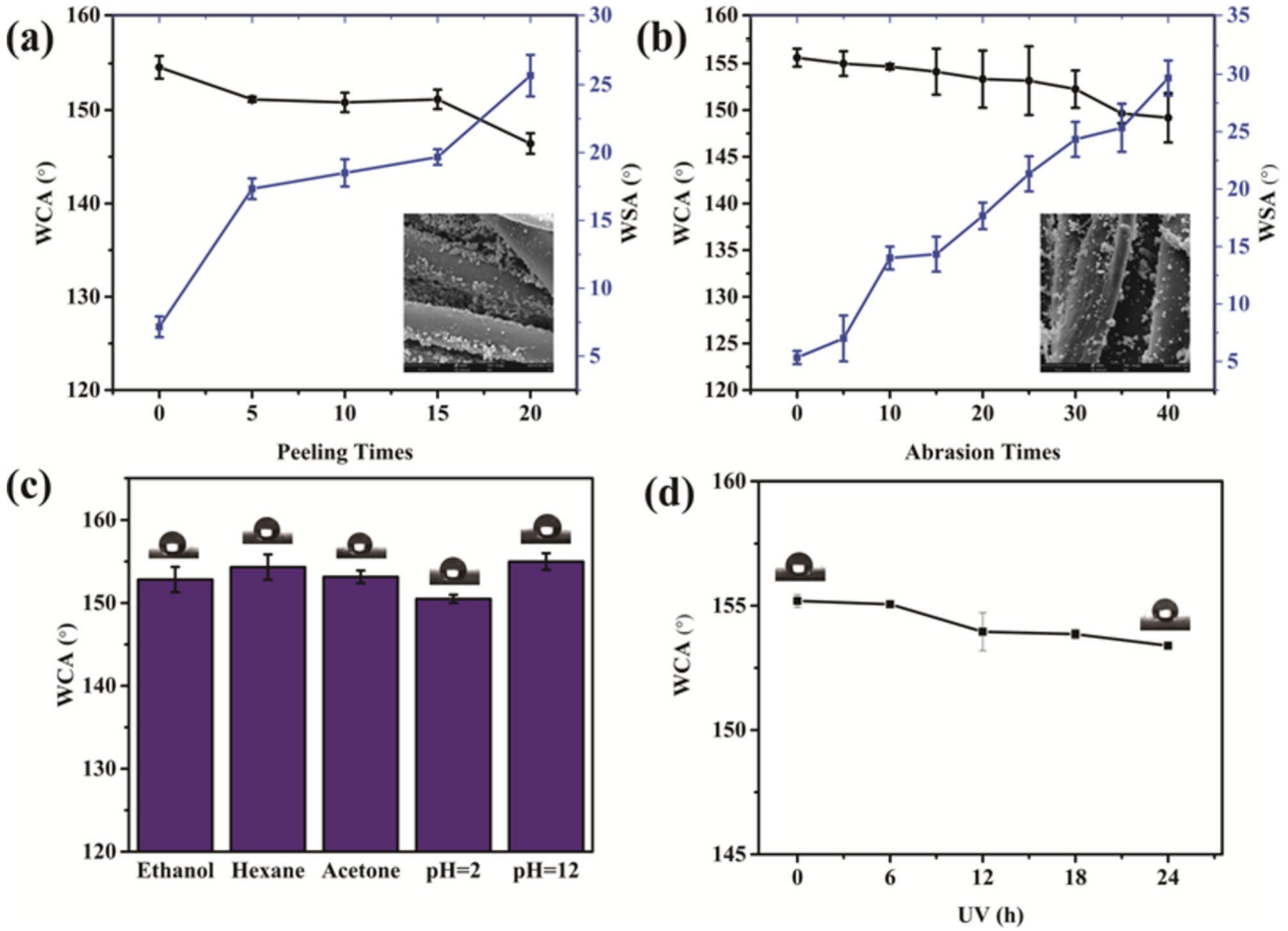

Fig. 8 **a** Friction test; **b** tape peeling test; **c** immersion test with different solutions; **d** UV aging test

they showed excellent durability against sandpaper abrasion, acid/alkali liquids, immersion in organic solutions, and UV irradiation. In addition, the RhB degradation efficiency could reach 63% after 6 h of UV irradiation and still be at 48% after 5 cycles of degradation. Janus particles can have two functions at the same time, such as hydrophobic and photocatalytic effects in this study, which is advantageous to achieve multifunctional coating and broaden the application in textiles.

Supplementary Information The online version contains supplementary material available at https://doi.org/10.1007/s12221-023-00451-x.

Acknowledgements This work was supported by Natural Science Foundation of Tianjin (grant Number 22JCQNJC01760), Basic Scientific Research Expenses of Tianjin Fire Science and Technology Research Institute of MEM (grant Number: 2023SJ17), the National Natural Science Foundation of China (grant number 11702187), 2021 Tianjin Postgraduate Research Innovation Project (grant number 2021YJSB235), Research Fund of China National Textile And Apparel Council (grant number 2022033), the Natural Science Foundation of Fujian (grant number 2022J05231). We would like to thank the Analytical &Testing Center of Tiangong University for the work related to surface morphology and chemical structure of the composite fabrics.

Author Contributions HW: resources, data curation, writing—original draft, and validation. HY: conceptualization and data curation. JW: investigation and data curation. TL: writing—review and editing, and formal analysis. J-HL: conceptualization, supervision, and validation. C-WL: conceptualization, resources, and validation.

Funding Natural Science Foundation of Tianjin, 22JCQNJC01760, Hongyang Wang, Tianjin Fire Research Institute of Ministry of Emergency Management, 2023SJ17, Hongyang Wang, Tianjin Postgraduate Research Innovation Project, 2021YJSB235, Ting-Ting Li, Research Fund of China National Textile And Apparel Council, 2022033, Junsheng Wang, Natural Science Foundation of Fujian Province, 2022J05231, Ching-Wen Lou.

Data Availability Statement Not applicable.

Declarations

Conflict of interest The authors declare that they have no known competing financial interests or personal relationships that could have appeared to influence the work reported in this paper.

References

1. C. Su, L. Zhou, C. Yuan, X. Wang, Q. Zhao, X. Zhao, and G. Ju, *Composites Science and Technology*, **231** (2023).
2. M. Luo, X. Sun, Y. Zheng, X. Cui, W. Ma, S. Han, L. Zhou, and X. Wei, *Applied Surface Science*, **609** (2023).
3. X.J. Guo, D. Zhang, C.H. Xue, B.Y. Liu, M.C. Huang, H.D. Wang, X. Wang, F.Q. Deng, Y.P. Pu, Q.F. An, ACS Appl. Mater. Interfaces **15**, 4612 (2023)
4. C.N.W. Barthlott, Planta **202**, 1 (1996)
5. J. Z. Zhenrui Yang , Wentao Zhang , Qin Zhou , Jiayuan Shen , Yi Huang *Journal of Cleaner Production*, **382** (2017).
6. X. Xia, J. Liu, Y. Liu, Z. Lei, Y. Han, Z. Zheng, and J. Yin, *Coatings*, **13** (2023).
7. S. L. Lin Feng, Yingshun Li, Huanjun Li, Lingjuan Zhang, Jin Zhai, Yanlin Song, Biqian Liu, Lei Jiang,* and Daoben Zhu, *Adv. Mater.*, **14**, 1857 (2002).
8. Y. Cao, Y. Lu, N. Liu, Y. Li, P. Wang, C. Dai, and Y. Wei, *Surfaces and Interfaces*, **32** (2022).
9. Y. Li, S. Chen, M. Wu, J. Sun, Adv. Mater. **26**, 3344 (2014)
10. M. H. Abd Aziz, M. H. D. Othman, J. R. Tavares, M. A. B. Pauzan, M. Tenjimbayashi, A. W. Lun, N. H. Alias, A. F. Ismail, M. A Rahman, and J. Jaafar, *Applied Surface Science*, **598** (2022).
11. J. Wang, Y. Zhang, and Q. He, *Separation and Purification Technology*, **306** (2023).
12. D. Wei, J. Wang, Y. Liu, D. Wang, S. Li, and H. Wang, *Chemical Engineering Journal*, **404** (2021).
13. Z. Hu, F. Ma, L. Liu, Z. Zeng, J. Yi, and Q. Li, *Progress in Organic Coatings*, **168** (2022).
14. T.L. Chen, C.Y. Huang, Y.T. Xie, Y.Y. Chiang, Y.M. Chen, H.Y. Hsueh, ACS Appl. Mater. Interfaces **11**, 40875 (2019)
15. G. Wang, A. Li, K. Li, Y. Zhao, Y. Ma, Q. He, J. Colloid Interface Sci. **588**, 175 (2021)
16. D. Liu, A. Wang, G. Wang, K. Gui, and M. Wang, *Materials & Design*, **210** (2021).
17. J. li, L. Xu, X. Yuan, H. Pan, L. Wang, Y. Shen, and K. Li, *Colloids and Surfaces A: Physicochemical and Engineering Aspects*, **651** (2022).
18. X. Jiao, M. Li, X. Yu, S. Yang, and Y. Zhang, *Chemical Engineering Journal*, **446** (2022).
19. W. Xu, L. Xu, H. Pan, K. Li, J. Li, L. Wang, Y. Shen, Y. Liu, T. Li, Cellulose **29**, 4021 (2022)
20. M. Zhang, S. Jiang, F. Han, H. Chen, N. Wang, L. Liu, L. Liu, Cellulose **29**, 3529 (2022)
21. Z.-Y. Deng, W. Wang, L.-H. Mao, C.-F. Wang, S. Chen, J. Mater. Chem. A **2**, 4178 (2014)
22. E. Pakdel, H. Zhao, J. Wang, B. Tang, R.J. Varley, X. Wang, Cellulose **28**, 8807 (2021)
23. Y. Yang, Z. Guo, Y. Li, Y. Qing, W. Wang, Z. Ma, S. You, and W. Li, *Separation and Purification Technology*, **282** (2022).
24. Y. Wang, S. Peng, X. Shi, Y. Lan, G. Zeng, K. Zhang, and X. Li, *Applied Surface Science*, **505** (2020).
25. M. Miyauchi, A. Nakajima, T. Watanabe, K. Hashimoto, Chem. Mater. **14**, 2812 (2002)
26. S. Wang, X. Feng, J. Yao, L. Jiang, Angew. Chem. Int. Ed. Engl. **45**, 1264 (2006)
27. X. Wang, H. Ding, C. Wang, R. Zhou, Y. Li, W. Li, and W. Ao, *Applied Surface Science*, **567** (2021).
28. A. Kirillova, C. Marschelke, A. Synytska, ACS Appl. Mater. Interfaces **11**, 9643 (2019)
29. S. Berger, L. Ionov, A. Synytska, Adv. Func. Mater. **21**, 2338 (2011)
30. T. Choisnet, D. Canevet, M. Salle, C. Lorthioir, L. Bouteiller, P. Woisel, F. Niepceron, E. Nicol, O. Colombani, ACS Nano **15**, 2569 (2021)
31. S. Gao, S. Song, J. Wang, S. Mei, J. Yuan, G. Liu, M. Pan, Colloids Surf. A **577**, 360 (2019)
32. J. Yang, X. Xu, Y. Liu, Y. Gao, H. Chen, and H. Li, *Colloids and Surfaces A: Physicochemical and Engineering Aspects*, **582** (2019).
33. Y. Bao, Y. Zhang, J. Ma, Nanoscale **12**, 16443 (2020)
34. Y. Ning, C. Wang, T. Ngai, Z. Tong, Langmuir **29**, 5138 (2013)
35. Y.H. Hwang, K. Jeon, S.A. Ryu, D.P. Kim, H. Lee, Small **16**, e2005159 (2020)
36. F. Chang, C.M. Vis, M. Bergmeijer, S.C. Howes, P.C.A. Bruijnincx, Chemsuschem **14**, 5328 (2021)
37. X. Zhang, Q. Fu, H. Duan, J. Song, H. Yang, ACS Nano **15**, 6147 (2021)
38. K. Panwar, M. Jassal, A.K. Agrawal, Particuology **19**, 107 (2015)
39. J. Zimmermann, S. Seeger, F.A. Reifler, Text. Res. J. **79**, 1565 (2009)
40. L. Li, X. Chen, X. Xiong, X. Wu, Z. Xie, Z. Liu, Ceram. Int. **47**, 2678 (2021)
41. U. Mahanta, M. Khandelwal, and A. S. Deshpande, *Applied Surface Science*, **576** (2022).
42. Y. Zhang, T.-T. Li, B.-C. Shiu, J.-H. Lin, and C.-W. Lou, *Applied Surface Science*, **584** (2022).
43. W. Ma, Y. Ding, Y. Li, S. Gao, Z. Jiang, J. Cui, C. Huang, and G. Fu, *Journal of Membrane Science*, **634** (2021).
44. L. Zong, Y. Wu, X. Li, B. Jiang, J. Coat. Technol. Res. **18**, 1245 (2021)
45. L. Zhang, L. Rao, P. Wang, Z. Shi, and P. Wang, *Applied Surface Science*, **536** (2021).
46. H. Huang, R. Shi, X. Zhang, J. Zhao, C. Su, T. Zhang, Angew. Chem. Int. Ed. Engl. **60**, 22963 (2021)
47. X. Hu, H. Zhang, Y. Wang, B.-C. Shiu, J.-H. Lin, S. Zhang, C.-W. Lou, and T.-T. Li, *Chemical Engineering Journal*, **450** (2022).